AQUA
Water Infrastructure, Ecosystems and Society



IWA PUBLISHING

 AQUA — Water Infrastructure, Ecosystems and Society Vol 73 No 6, 1164 doi: 10.2166/aqua.2024.326

# Mass transfer of $CO_2$ gas pocket in horizontal pipe flow

Linjiang Guo[a], Lei Fang[a], Pengcheng Li[b,c] and Yiyi Ma[a,*]

[a] Department of Civil Engineering, Zhejiang University, Hangzhou 310058, China
[b] Department of Civil and Environmental Engineering, University of Alberta, Edmonton T6G 1H9, Canada
[c] Ecofish Research, Vancouver, Canada
*Corresponding author. E-mail: yiyima@zju.edu.cn

YM, 0000-0003-3874-0306

## ABSTRACT

The mass transfer from a stagnant $CO_2$ gas pocket to the flowing water in a horizontal pipe was investigated experimentally, considering the application of pH adjustment by injecting gaseous $CO_2$ for raw water in water treatment industries. In the experiments, the variation of the $CO_2$ gas pocket volume and the corresponding pH values of the pipe flow with time under different conditions were recorded. The mass transfer coefficient of the $CO_2$ gas pocket in the pipe flow was then calculated. The results showed that the injection of gaseous $CO_2$ into the pipe flow could effectively adjust the pH. The volume of the $CO_2$ gas pocket decreased exponentially. Different from most studies on bubble mass transfer, it was found that the ambient $CO_2$ concentration could not be neglected in this study due to the large volume of the gas pocket and the restricted space in the pipe. The mass transfer coefficient increased with the increasing ratio of the $CO_2$ injection rate to the water flow rate and exhibited a sharp reduction as the volume of the $CO_2$ gas pocket decreased by about 80%. The outcomes of this paper can contribute to a better understanding of gas bubble mass transfer in pipe flows.

**Key words:** $CO_2$ gas pocket, gas volume, mass transfer coefficient, pH, pipe flow

## HIGHLIGHTS

- The mass transfer of a large $CO_2$ gas pocket in the horizontal pipe flow was investigated, which has been hardly reported before.
- During mass transfer processes, the pH variation of the pipe flow could be divided into three regimes, and the volume of the gas pocket was reduced exponentially.
- The $CO_2$ concentration in the pipe flow is important to mass transfer due to the large volume of the gas pocket and the restricted space in the pipe.

## 1. INTRODUCTION

Gas–liquid mass transfer occurs when the gas solubility in the liquid phase is lower than the saturation solubility, or when the partial pressure of the gaseous solute in the liquid phase is higher than that in the gas phase (Cheng *et al.* 2008). The bubble mass transfer phenomenon can be observed in nature like river reoxygenation and industrial processes (Shimizu *et al.* 2000). Recently, algae blooms caused by eutrophication have become increasingly serious, and the pH of raw water has risen sharply as a consequence (Liu *et al.* 2016). Injecting gaseous $CO_2$ into transportation pipelines has been proposed as a method of pH control for raw water in water supply engineering. Since this method is considered economical, environmentally friendly, safe, stable, and efficient in the removal of organic matter, it is receiving increasing attention. Although the mass transfer of small bubbles or bubble swarms moving in still/flowing fluid has been extensively studied, the understanding of the mass transfer from large gaseous $CO_2$ pockets to flowing water in a pipe with restricted space is relatively limited. Investigating the features of such mass transfer processes is crucial for both industrial applications and the development of bubble mass transfer theories.

It has been commonly recognized that the mass transfer between a bubble and its surrounding water is determined by the bubble–water interfacial area, bubble residence time, mass transfer coefficient, and concentration difference. The rate of mass transfer can be written as: $dM/dt = -K_L A(C_s - C)$, where $M$ is the gas mass inside the bubble, $t$ is time, $K_L$ is the mass transfer

coefficient, $A$ is the bubble–water interfacial area, $C$ is the dissolved gas concentration in water, and $C_s$ is the liquid-phase equilibrium concentration under the local partial pressure of the gas. The calculation of $K_L$ is one of the key issues in bubble mass transfer. Over the last hundred years, researchers have proposed different theories for $K_L$ depending on how the solute is transferred from the gas phase to the liquid phase. The most recognized models are the two-film theory proposed by Whitman (1923), the percolation theory by Higbie (1935), and the surface renewal model by Danckwerts (1951). The three classical mass transfer theories have provided a clear interpretation of the mass transfer processes and laid a solid foundation for subsequent studies.

Based on the three classical mass transfer theories, there have been extensively modified models developed through experimental studies and numerical simulations. Kubaczka & Bandrowski (1991) improved the two-film theory by including the variation of mass transfer coefficient with temperature and concentration in the model. Ma & Yu (1998) proposed the three-film theory of gas–liquid mass transfer as an improvement of the two-film theory by considering three resistance films for gas–liquid mass transfer. Perlmutter (1961) adjusted the surface renewal model by considering the flow of fluid elements from the liquid bulk to the interface as a tandem process. Models developed by combining two or three of the classical models have also been reported. For example, Hanratty (1956) proposed the film-penetration theory which was a combination of the two-film theory and the penetration theory.

The process of bubble mass transfer is significantly influenced by the bubble characteristics and the properties of the surrounding fluid. Cai *et al.* (2012) reported that as the bubble equivalent diameter increased, the bubble agglomeration behavior decreased, leading to an increase in both the gas–liquid interface area and the gas–liquid mass transfer coefficient. Motarjemi & Jameson (1978) experimentally verified that a single $CO_2$ bubble with a diameter of 2–3 mm had the highest mass transfer efficiency, compared with the bubbles of other sizes. Also, the bubble shape affects the contact area between the fluid and the bubble, which in turn affects the mass transfer efficiency (Xie *et al.* 2022). In addition, the flow velocity, viscosity, and the degree of turbulence of the fluid can influence the bubble mass transfer efficiency (Shaw & Hanratty 1977; Stoodley *et al.* 1997; Song *et al.* 2017). The liquid-phase flow rate affects the thickness of the diffusion boundary layer on the membrane surface, which, in turn, affects the gas transfer efficiency (Wang *et al.* 2016). Yang *et al.* (2022) found that the mass transfer coefficient increased with the liquid flow rate through both experiments and numerical modeling.

However, most of the existing studies focus on the mass transfer of a single bubble or bubble swarms moving freely in a stationary or flowing water body (Nock *et al.* 2016; Li *et al.* 2020). The situation of bubble mass transfer in the pipe flow is more complex due to the different dynamic features of gas/water flow under the constraint of the pipe wall, which has hardly been studied. Also, many previous studies have analyzed the bubble mass transfer process by assuming that the surrounding dissolved gas concentration is zero, considering the large space of the ambient fluid. The knowledge on the mass transfer of large gas pockets in a constrained space is limited, where the surrounding dissolved gas concentration is not negligible. This study experimentally investigated the mass transfer of a large stagnant $CO_2$ gas pocket in a horizontal pipe with flowing water. In the experiments, gaseous $CO_2$ was injected into the horizontal pipe until a stagnant $CO_2$ gas pocket was formed. The pH variation in the pipe under different water flow rates and $CO_2$ injection rates was measured and analyzed. The corresponding $CO_2$ gas pocket volume change was also recorded. The mass transfer coefficients were then calculated for each experimental condition, and their variation with the $CO_2$ injection rate and the water flow rate was also investigated.

## 2. EXPERIMENTS

The schematic of the experimental setup in this study is shown in Figure 1, which mainly consists of a horizontal pipe with an internal diameter of 50 mm and a length of 5,000 mm, a water pump, a $CO_2$ storage cylinder, a large water tank, and valves. Water was supplied from the large tank by the pump through a pipe of 50 mm diameter and 1.5 m length before entering the test horizontal pipe for a stabilized inflow. The gas and water flow rates ($Q_a$ and $Q_w$) were controlled by valves that were labeled as (1) and (2) in Figure 1.

In the experiments, the $CO_2$ flow rate was measured by a rotameter (LZB-3WB6, manufactured by Nanjing Dahua, Inc.), and the water flow rate was recorded by a flow meter (Lux-dn15, manufactured by Baoji Huaqiang, Inc.). The changes in pH were measured by a pH meter (MIK-Ph160, manufactured by Hangzhou Asmik) placed 0.5 m away from the end of the pipe (see Figure 1). These measurements were taken at a frequency of 0.2 Hz. The real-time pH data (i.e., pH – $t$ curves) were recorded by the Asmik software on the computer. The pressure in the pipe was measured by a pressure gauge, as shown in Figure 1. The appearance of the $CO_2$ gas pocket inside the pipe was recorded by five cameras (SONY HDR-CX405).

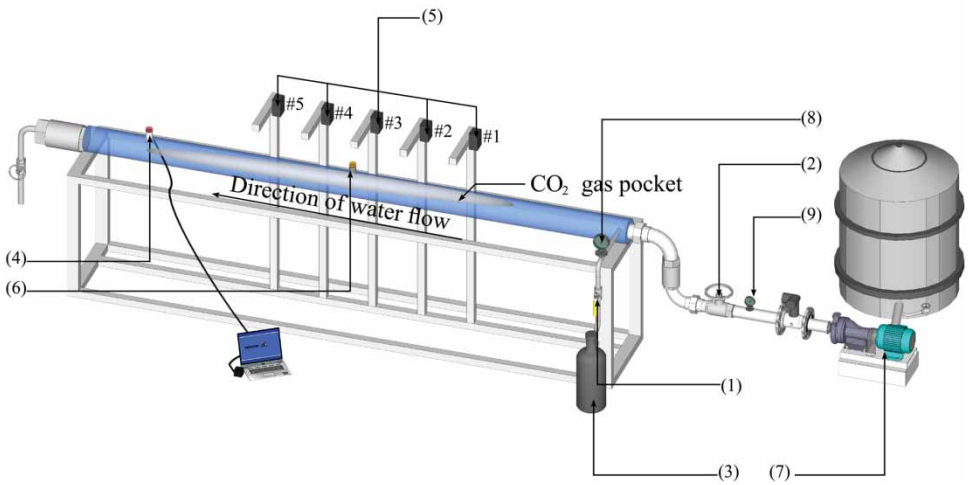


**Figure 1** | Schematic of the experimental setup. (1) Gas valve, (2) water valve, (3) $CO_2$ storage cylinder, (4) pH meter, (5) cameras, (6) pitot tube, (7) water pump, (8) gas flow meter, and (9) water flow meter.

These cameras, named Camera #1, #2, #3, #4, and #5, were placed at 0.5 m intervals along the pipe in the direction of water flow (see Figure 1). The dimensions of the gas pocket were then obtained from the camera video images. The temperature of water was measured by a contact thermocouple thermometer (KOMAX, manufactured by Hangzhou Komax, Inc.). The details of the installation of the instruments are presented in Figure 1.

Before the experiment, the desired water flow rate was first achieved by adjusting the valve, and the pipe was filled with water. The glass electrode was then inserted into the water and started to record the pH values. Following that, all the cameras were turned on, and the illumination device was opened. The start of the experiment was marked as the moment of starting the gaseous $CO_2$ injection, i.e., $t = 0$ s. The pH dropped first as $CO_2$ was continuously injected into the water, while it got steady after a certain period. The gas injection was then stopped, and a $CO_2$ gas pocket was formed in the pipe. Subsequently, the size of the $CO_2$ gas pocket kept decreasing due to the dissolution of gaseous $CO_2$ . The experiment ended once the $CO_2$ gas pocket disappeared. The change in the gas pocket volume and the variation of pH in water were recorded simultaneously. The experiments were conducted under nine different conditions, as listed in Table 1. The flow rate was 15.6–24.7 L/min, the corresponding pipeline flow velocity was 0.13–0.18 m/s, and the corresponding $Re = 7.3 \times 10^3$–$1.01 \times 10^4$. The initial pH of the raw water used in this experiment was around 8.2, and the water temperature was 25 °C.

**Table 1** | Experimental conditions

| Case | Water flow rate $Q_w$ (L/min) | $CO_2$ flow rate $Q_a$ (L/min) | Duration of $CO_2$ injection $\Delta t$ (s) | Total injected $CO_2$ volume $V_a = Q_a \Delta t$ (L) |
|---|---|---|---|---|
| 1 | 18.1 | 3.0 | 121 | 6.1 |
| 2 | 18.1 | 4.0 | 122 | 8.1 |
| 3 | 18.0 | 7.0 | 123 | 14.3 |
| 4 | 15.6 | 6.0 | 105 | 10.5 |
| 5 | 18.1 | 6.0 | 103 | 10.3 |
| 6 | 24.7 | 6.0 | 106 | 10.6 |
| 7 | 18.1 | 6.0 | 60 | 6.0 |
| 8 | 18.1 | 6.0 | 80 | 8.0 |
| 9 | 18.1 | 6.0 | 120 | 12.0 |

## 3. RESULTS AND DISCUSSION

### 3.1. Variation of the $CO_2$ gas pocket volume

The reproducibility of the experimental results was checked first. The experiment under the condition of $Q_a = 8$ L/min, $Q_w = 15.6$ L/min, and $CO_2$ injection time $t = 0$–120 s (i.e., the duration of $CO_2$ injection $\Delta t = 120$ s) was repeated four times to see the consistency of the pH variation in each test. The results are shown in Figure 2, which indicates good reproducibility. Another set of experiments was conducted with gaseous $N_2$, which is insoluble in water, to exclude the possibility of gas pocket volume reduction caused by turbulent shear in flowing water. When replacing $CO_2$ with $N_2$, the gas pocket volume maintained the same size during the experiment (see Figure 3(a)), and the pH of water remained constant. Therefore, in the experiments, the effects of turbulent shear on the volume of the $CO_2$ gas pocket were negligible, and the volume reduction was mainly due to the mass transfer.

The morphological characteristics of the $CO_2$ gas pocket recorded by Camera #1 at different time points, specifically $t = 120$ s, $t = 240$ s, and $t = 420$ s, are shown in Figure 3(b). The experimental condition is Case 2, with the water flow rate $Q_w = 18.1$ L/min, the $CO_2$ injection rate $Q_a = 4$ L/min, the duration of $CO_2$ injection $\Delta t = 122$ s (i.e., $CO_2$ injection stopped at $t = 122$ s), and the total injected $CO_2$ volume $V_a = 8.14$ L. From Figure 3(b), the volume of the gas pocket keeps decreasing since the $CO_2$ injection stops. Qualitatively, the gas pocket disappears from the field of view of Camera # 5 at $t = 150$ s and from the field of view of Camera # 4 at $t = 210$ s. It can only be observed in the field of view of Camera # 1 starting from $t = 240$ s.

In this study, the volume of the gas pocket was determined from the camera video images. MATLAB was used to extract single images from the camera videos, and Photoshop was applied to quantify the dimensions of gas pockets from the images. The estimation of the gas pocket volume is as follows. During a short period after $CO_2$ injection stops, the gas pocket morphology is relatively regular along the pipe, as shown in Figure 3(b) ($t = 120$ s). Considering the long shape of the gas pocket, the air–water interface of the gas pocket is approximated to be flat, as illustrated in Figure 4. Scaled from the actual pipe diameter $D = 50$ mm, the actual width ($W$, unit: mm) of the gas pocket can be estimated by the following equation:

$$\frac{w}{d} = \frac{W}{D} \tag{1}$$

where $w$ and $d$ are the graphic gas pocket width and pipe diameter measured from the video images (unit: pixel). Furthermore, based on the actual width of the gas pocket $W$, and the known pipe radius $r$, the angle $\alpha$ (in degree) in the pipe cross-section (as shown in Figure 4(a)) can be calculated through

$$W = 2r\sin\left(\frac{\alpha}{2}\right) \tag{2}$$

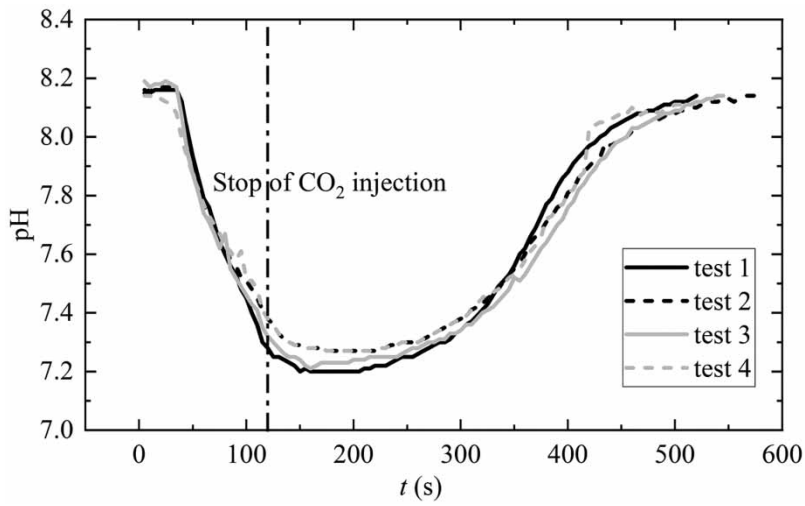


**Figure 2** | Reproducibility tests of experiments ($Q_w = 15.6$ L/min, $Q_a = 8$ L/min, $\Delta t = 120$ s).

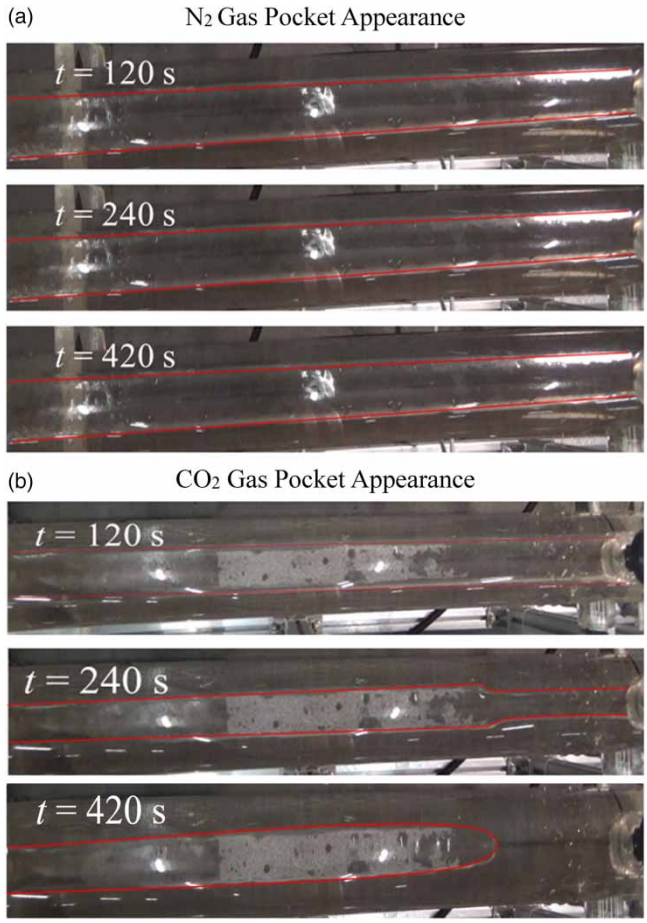


**Figure 3** | Variations of (a) $N_2$ gas pocket and (b) $CO_2$ gas pocket in the pipe at different moments.

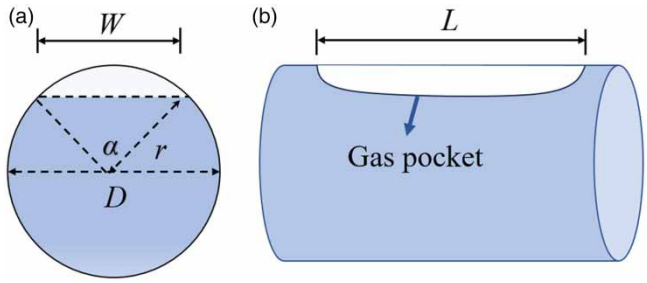


**Figure 4** | Gas pocket volume estimation: (a) front view and (b) lateral view.

The cross-sectional area of the gas pocket $S$ can then be estimated as follows:

$$S = \frac{\alpha}{360^\circ}\pi r^2 - \frac{1}{2}r^2 \sin\alpha \tag{3}$$

The volume of the gas pocket $V_1$ is then obtained as follows:

$$V_1 = S \times L \tag{4}$$

where $L$ is the length of the gas pocket, as shown in Figure 4. As time passes, the gas pocket starts to retract from the side near the pH meter and gradually turns into an irregular shape, as shown in Figure 3(b) ($t = 420$ s). The gas pocket can be simplified as two parts for volume estimation, including an ellipsoid and the remaining part like that described in $V_1$ above. The volume calculation is then conducted for the two parts individually. The second part is approximated as a 1/4 ellipsoid. The volume of the second part $V_2$ is then obtained as follows:

$$V_2 = \frac{\pi abW}{6} \tag{5}$$

where $a$ and $b$ are the lengths of the major and minor axes. Figure 5 shows the variation of gas pocket volume $V$ with time right after gas injection cessation under different conditions. Based on correlation, the variation of gas pocket volume with time follows exponential law, as shown in Figure 5. From Figure 5(a) and 5(b), the increase in the water flow rate accelerates the rate of gas pocket volume reduction. Additionally, comparing Figure 5(c) and 5(d), a greater amount of injected $CO_2$ can lead to a faster rate of volume reduction, which is due to the larger gas–liquid interfacial area and potentially a larger mass transfer coefficient due to more turbulent conditions near the bubble–water interface.

### 3.2. Variations of pH in the pipe flow

The variations of pH in the pipe flow under different conditions of water/$CO_2$ flow rates and $CO_2$ injection duration are shown in Figure 6. The pH change process can be divided into three regimes, including the lowering regime, the steady regime, and the recovery regime, as labeled in Figure 6. At the beginning of the experiment, $CO_2$ dissolves into water and the pH of water decreases rapidly, which is the lowering regime. As $CO_2$ continues being injected, the pH changes little and there is a plateau on the pH curve, which is the steady regime. When the $CO_2$ injection is stopped, the $CO_2$ gas pocket in the pipe continues to react with the water flow, but the amount of H ions ionized by the reaction between $CO_2$ and water is reduced, which, in turn, leads to a gradual rise in pH. It is the recovery regime.

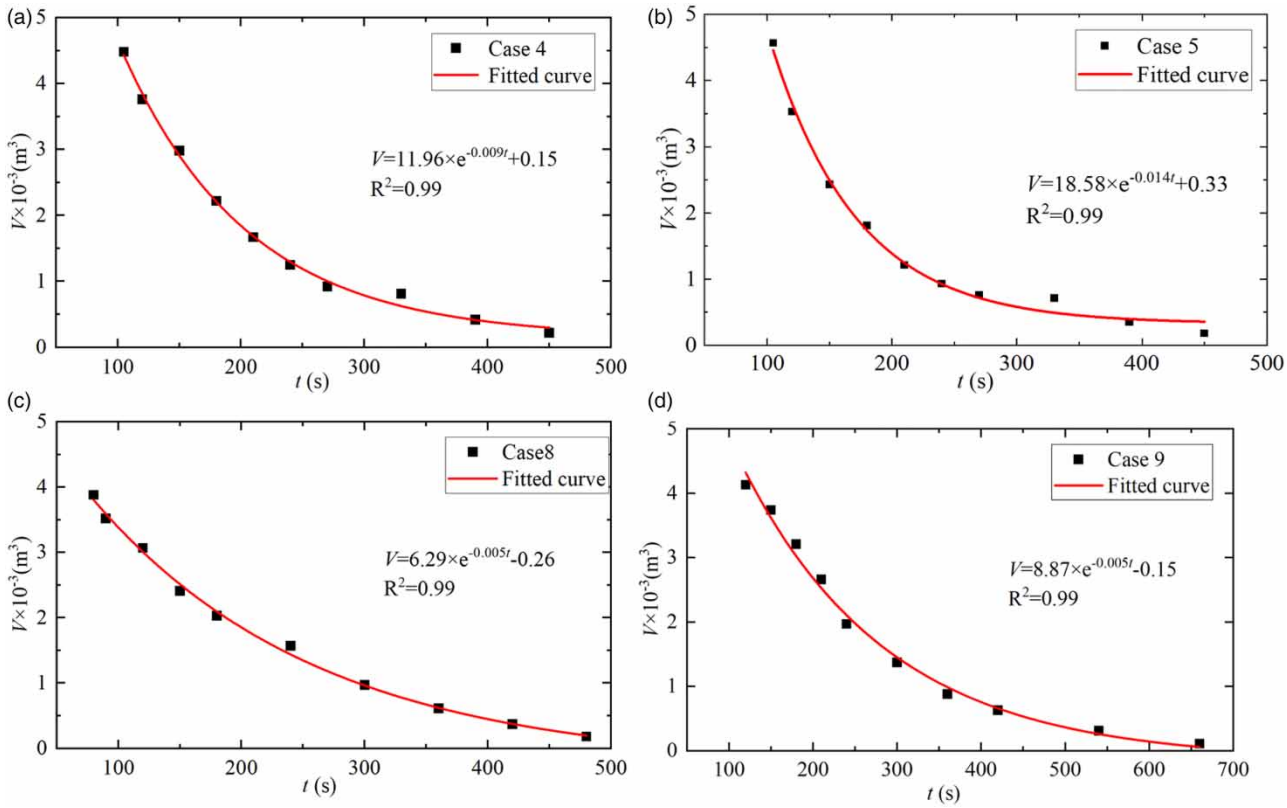


**Figure 5** | Variations of the $CO_2$ gas pocket volume with time: (a) Case 4, $Q_w = 15.6$ L/min, $Q_a = 6$ L/min, $\Delta t = 105$ s; (b) Case 5, $Q_w = 18.1$ L/min, $Q_a = 6$ L/min, $\Delta t = 103$ s; (c) Case 8, $Q_w = 18.1$ L/min, $Q_a = 6$ L/min, $\Delta t = 80$ s; and (d) Case 9, $Q_w = 18.1$ L/min, $Q_a = 6$ L/min, $\Delta t = 120$ s.

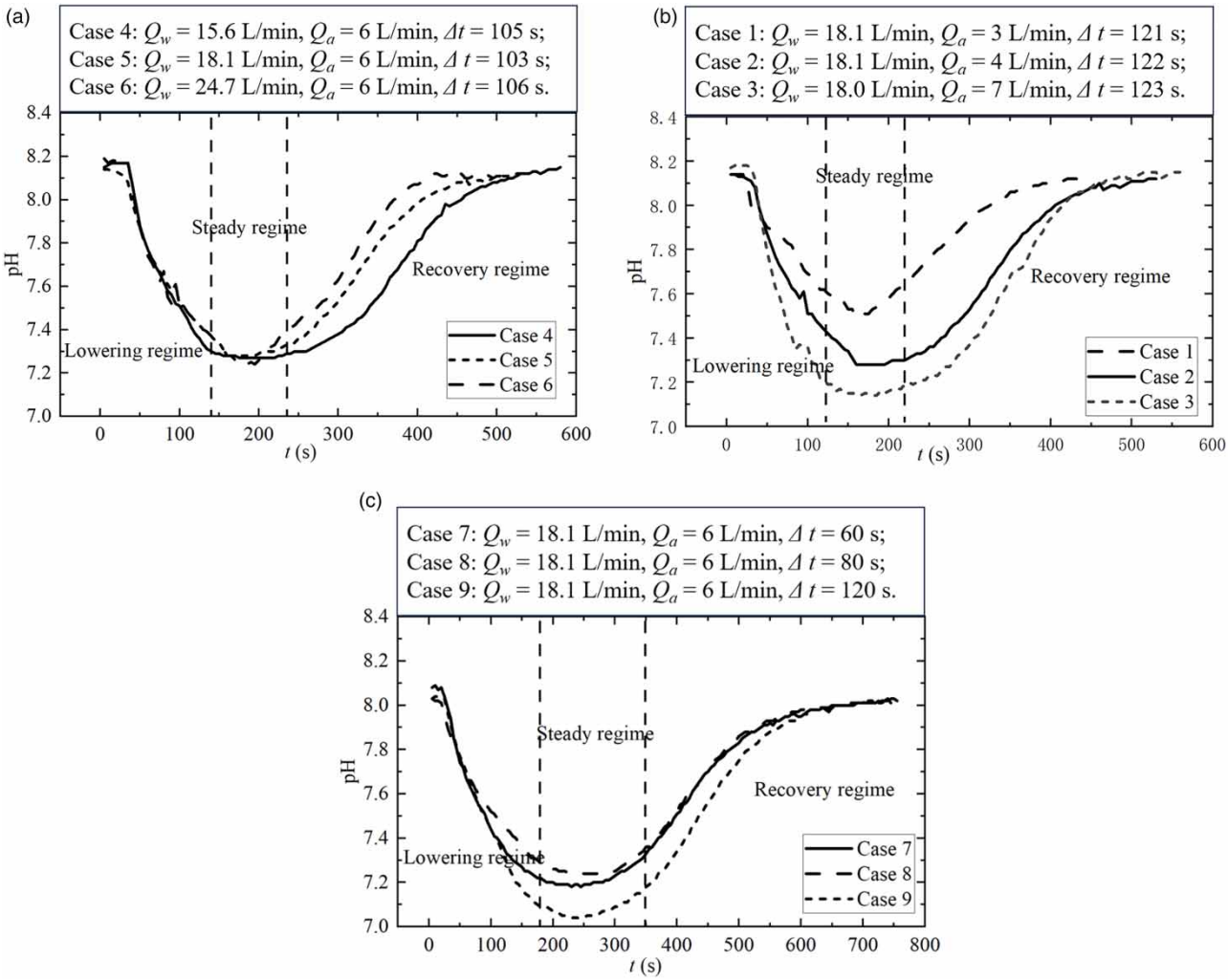


**Figure 6** | Variations of pH in water with time: (a) same total amount of injected gaseous $CO_2$ but different water flow rates; (b) same water flow rate but different gaseous $CO_2$ flow rates; and (c) same $CO_2$ and water flow rates but different injection durations.

Figure 6(a) shows the pH curve under different water flow rates but the same $CO_2$ flow rate and injection duration. Under the water flow rate $Q_w = 24.7$ L/min, the time for water pH goes back to the initial value (about 8.2), i.e., pH recovery time, is $t = 380$ s. When the water flow rate $Q_w = 15.6$ L/min, the pH recovery time is $t = 500$ s. The results show that the rate of pH decrease is almost the same in the lowering regime. At higher water flow rates, $CO_2$ reacts with water at a faster rate and the corresponding pH recovery time is shorter. Figure 6(b) shows the pH curve under different $CO_2$ injection rates but with the same $CO_2$ injection time and the water flow rate. According to the experimental results, a higher $CO_2$ injection rate leads to a faster reduction of water pH. After stopping the $CO_2$ injection, the water pH returns to its initial value within a similar duration in these cases, approximately $t = 440$ s. Figure 6(c) shows the pH change curve under the same $CO_2$ injection rate and the water flow rate but different injection durations. It is seen that the decrease in water pH is more significant as the injection duration increases. After stopping the $CO_2$ injection, there is a long plateau on the pH curve. Subsequently, the pH gradually rises to its initial value at around $t = 600$ s. In addition, a longer $CO_2$ injection duration results in a greater pH recovery rate.

### 3.3. Mass transfer coefficient

The mass transfer coefficient from the $CO_2$ gas pocket to the flowing water is calculated below. Assume that the $CO_2$ in the gas pocket follows the ideal gas law

$$PV = nRT \tag{6}$$

where $P$ is the gas pressure, $T$ is the temperature, $R$ is the ideal gas constant, and $n$ is the amount of gas substance. From Equation (6), the volume of the $CO_2$ gas pocket varies with the pressure and the amount of substance at a given temperature. From the experiments, when there was a gas pocket, the pressure in the pipe slightly decreased, indicating that the influence of the gas pocket on the pressure in the pipe was limited. Therefore, when calculating the mass transfer coefficient in this study, the value of $P$ in Equation (6) is considered constant in each test.

The amount of $CO_2$ transferred from the gas pocket to the water is

$$dM = M_m dn \tag{7}$$

where $M_m$ is the molar mass of $CO_2$. Combining the mass transfer equation $dM/dt = -K_L A(C_s - C)$, Equation (6) and Equation (7), it yields

$$M_m \frac{P}{RT}\frac{dV}{dt} = -K_L A(C_S - C) \tag{8}$$

$CO_2$ is present in water in the following reactions:

$CO_2$ hydrolysis reaction: $CO_2 + H_2O \rightleftharpoons H_2CO_3$ (9)

Carbonic acid primary ionization: $H_2CO_3 \rightleftharpoons HCO_3^- + H^+$ (10)

Carbonic acid secondary ionization: $HCO_3^- \rightleftharpoons CO_3^{2-} + H^+$ (11)

As the water pH is less than 8.3, only the primary ionization equilibrium of carbonic acid needs to be considered (Stoodley *et al.* 1997). Thus, in this study, only the primary ionization of carbonic acid was considered. The equilibrium constant for the reaction of $CO_2$ with water is

$$K = \frac{c(H_2CO_3)}{c(CO_2)} \tag{12}$$

The ionization constant for carbonic acid is

$$K_1 = \frac{(c(HCO_3^-)c(H^+))}{c(H_2CO_3)} \tag{13}$$

After the injection of $CO_2$, the pH of the flowing water in the pipe decreased sharply. Based on the reduction in pH, i.e., the difference between the concentration of H ions obtained from the reaction of $CO_2$ with water and the concentration of H ions in the raw water, $c(H^+)$ in Equation (9) can be calculated. The equilibrium constant $K$ for the reaction between $CO_2$ and water and the carbonic acid ionization constant $K_1$ are both obtained from Soli & Byrne (2002). Based on Equations (12) and (13), as well as the pH data measured in the experiments, $c(CO_2)$ (i.e., $C$ in Equation (8)) is then obtained. Additionally, $C_s$ can be calculated from Henry's Law, and the gas–liquid interfacial area $A$ can be estimated from the video images. Thus, $K_L$, under each experimental condition, can be calculated from Equation (8), as plotted in Figure 7(a). In this study, the Sherwood number was also applied to measure the mass transfer efficiency of the $CO_2$ gas pocket, which is dimensionless and defined as $Sh = K_L d_e / D_L$ ($d_e$ = characteristic length of the gas pocket, $D_L$ = liquid diffusivity of $CO_2$). The values of Sh under different conditions are plotted in Figure 7(b).

From Figure 7, the variations of mass transfer coefficients under all the experimental conditions show similar patterns. The mass transfer coefficient first increases but then decreases after a certain period. The increase in the mass transfer coefficient can be due to the fact that at the beginning of the mass transfer, the resistance at the gas–liquid interface is low and the gas molecules can dissolve rapidly into the liquid phase (Mavroudi *et al.* 2006). As the mass transfer process continues, the concentration gradient at the gas–liquid interface is reduced, and the driving force for mass transfer is weakened, which leads to a decrease in the mass transfer rate. Comparing Cases 2 and 3, under the same water flow rate, the increase in the $CO_2$ injection rate, i.e., the increase in the ratio of the $CO_2$ flow rate to the water flow rate in the pipeline, results in the increase in the mass

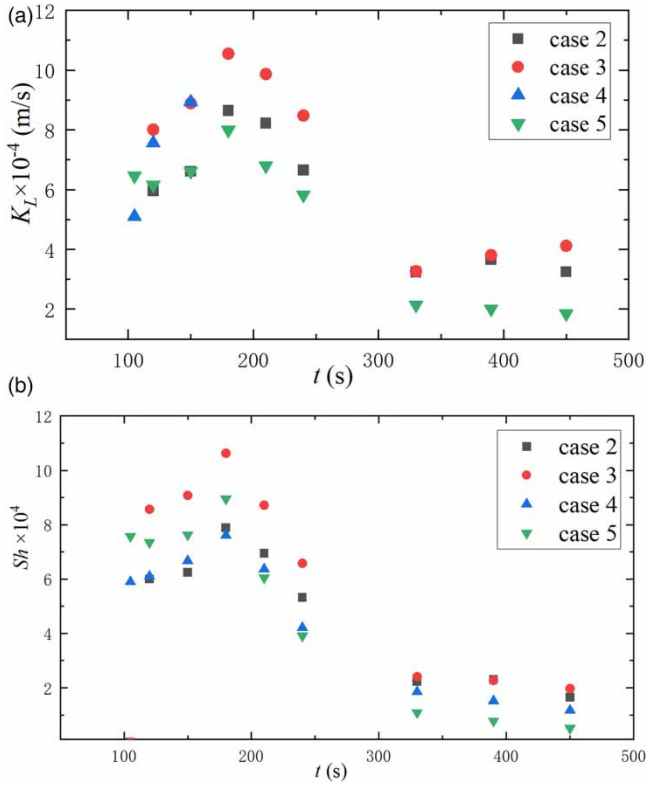


**Figure 7** | Variations of (a) mass transfer coefficient $K_L$ and (b) Sherwood Number Sh with time (Case 2: $Q_w = 18.1$ L/min, $Q_a = 4$ L/min, $\Delta t = 121$ s; Case 3: $Q_w = 18.0$ L/min, $Q_a = 7$ L/min, $\Delta t = 123$ s; Case 4: $Q_w = 15.6$ L/min, $Q_a = 6$ L/min, $\Delta t = 105$ s; Case 5: $Q_w = 18.1$ L/min, $Q_a = 6$ L/min, $\Delta t = 103$ s).

transfer efficiency. It is due to the enlarged gas–liquid contact area, as reported by Farajzadeh *et al.* (2007). Based on the results of Cases 4 and 5, with the same $CO_2$ flow rate and injection duration, the mass transfer coefficient increases with the water flow rate at the beginning of the mass transfer process. It is because an increase in the water flow rate leads to a higher degree of turbulence and promotes the mass transfer process. As the mass transfer process is close to the end, the water flow rate has little effect on the mass transfer coefficient. The reason is that when the volume of the $CO_2$ gas pocket is reduced to a certain level, the concentration of $CO_2$ in water is much lower compared to that at the beginning of the mass transfer. The mass transfer driving force is weakened, so the effect of the water flow rate on the mass transfer coefficient becomes less significant.

Figure 8 shows the variations of mass transfer coefficients and the corresponding changes in pH and $CO_2$ gas pocket volume. The results validate the close relationship between the mass transfer coefficient and the $CO_2$ concentration in water. After that, as the water pH rises, the $CO_2$ mass transfer coefficient decreases. Comparing the mass transfer coefficient and the change in $CO_2$ gas pocket volume, it shows that when the gas pocket volume is reduced by about 80% of its original size, the mass transfer coefficient suffers a sudden decrease. The mechanism for this sudden reduction in the mass transfer coefficient needs to be further explored in future works.

## 4. CONCLUSIONS

In this paper, the mass transfer process of a large $CO_2$ gas pocket in the pipe flow was investigated, which can occur during the pH adjustment process of raw water in water supply engineering, and is also a phenomenon having been hardly studied experimentally before. The changes in pH, the volume of the $CO_2$ gas pocket, and the mass transfer coefficients under different water–gas conditions were recorded and analyzed. According to the experimental results, the ratio of the gaseous $CO_2$ injection rate to the water flow rate, the volume of the gas pocket, and the dissolved $CO_2$ concentration in the pipe flow all have large influences on the mass transfer process.

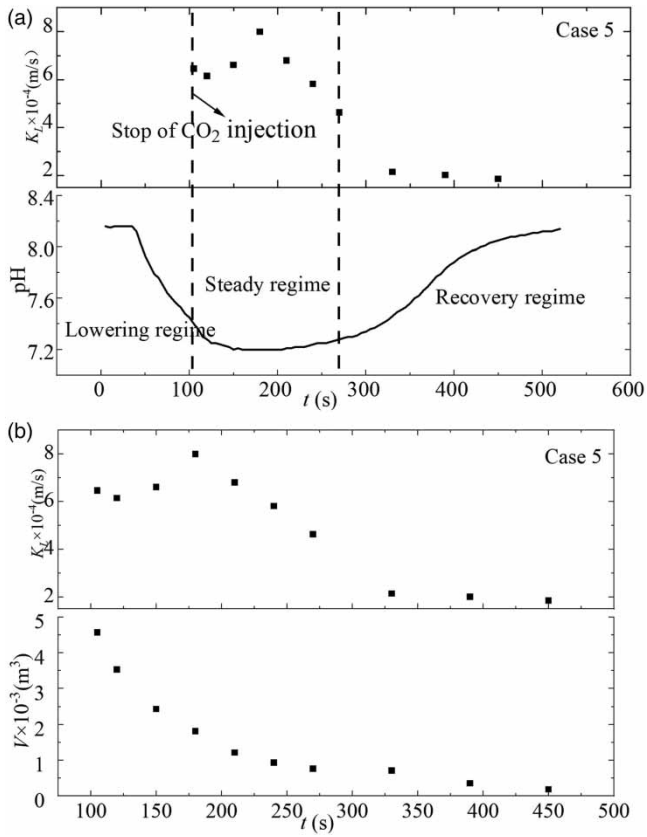


**Figure 8** | Variations of the mass transfer coefficient with (a) pH in the pipe flow and (b) the $CO_2$ gas pocket volume under the condition of Case 5: $Q_w = 18.1$ L/min, $Q_a = 6$ L/min, $\Delta t = 103$ s.

More specially, the injection of gaseous $CO_2$ into the pipe flow could effectively adjust the pH. The gas pocket volume was reduced approximately exponentially under all the experimental conditions. The pH change process could be divided into three regimes, including the lowering regime, the steady regime, and the recovery regime. The mass transfer coefficient of the $CO_2$ gas pocket in the steady regime was larger than that in the recovery regime. The results also validated the close relationship between the mass transfer coefficients and the variation of $CO_2$ concentration in the pipe flow due to the large volume of the gas pocket, which is different from many studies neglecting the ambient $CO_2$ concentration for simplified calculation. The mass transfer coefficient increased with the increasing ratio of the $CO_2$ injection rate to the water flow rate. The outcomes of this paper can contribute to a better understanding of gas bubble mass transfer in pipe flows and are meaningful for practical applications.

## ACKNOWLEDGEMENTS

The authors gratefully acknowledge financial support from the National Key R&D Program of China (Grant No. 2022YFC3202602), the Natural Science Foundation of Zhejiang Province (Grant No. LZJWZ23E090009), the National Natural Science Foundation of China (Grant No. 52300122).

## DATA AVAILABILITY STATEMENT

All relevant data are included in the paper or its Supplementary Information.

## CONFLICT OF INTEREST

The authors declare there is no conflict.

## REFERENCES


Cai, Z., Gao, Z., Bao, Y., Evans, G. M. & Doroodchi, E. 2012 Formation and motion of conjunct bubbles in glycerol–water solutions. *Industrial & Engineering Chemistry Research* **51** (4), 1990–1996.

Cheng, W., Liu, W., Hu, B. & Wan, T. 2008 Experimental study on gas-liquid two-phase flows in an aeration tank by using image treatment method. *Journal of Hydrodynamics* **20** (5), 650–655.

Danckwerts, P. 1951 Significance of liquid-film coefficients in gas absorption. *Industrial and Engineering Chemistry* **43** (6), 1460–1467.

Farajzadeh, R., Barati, A., Delil, H. A., Bruining, J. & Zitha, P. L. J. 2007 Mass transfer of $CO_2$ into water and surfactant solutions. *Petroleum Science and Technology* **25** (12), 1493–1511.

Hanratty, T. 1956 Turbulent exchange of mass and momentum with a boundary. *Aiche Journal* **2** (3), 359–362.

Higbie, R. 1935 The rate of absorption of a pure gas into a still liquid during short periods of exposure. *Transactions of the American Institute of Chemical Engineers* **31**, 365–389.

Kubaczka, A. & Bandrowski, J. 1991 Solutions of a system of multicomponent mass-transport equations for mixtures of real fluids. *Chemical Engineering Science* **46** (2), 539–556.

Li, P., Ma, Y. & Zhu, D. Z. 2020 Mass transfer of gas bubbles rising in stagnant water. *Journal of Environmental Engineering* **146** (8), 04020084.

Liu, J.-R., Xiao, F., Liu, X., Yang, R., Du, S. & Liu, Y. 2016 Coping strategies for abnormally elevated raw water pH in small water plants. *China Water Supply and Drainage* **32** (17), 48–50.

Ma, Y. & Yu, G. 1998 Theoretical study of gas-liquid interphase mass transfer. *Journal of Tianjin University* **4**, 123–127.

Mavroudi, M., Kaldis, S. P. & Sakellaropoulos, G. P. 2006 A study of mass transfer resistance in membrane gas–liquid contacting processes. *Journal of Membrane Science* **272** (1–2), 103–115. https://doi.org/10.1016/j.memsci.2005.07.025.

Motarjemi, M. & Jameson, G. 1978 Mass-transfer from very small bubbles – optimum bubble-size for aeration. *Chemical Engineering Science* **33** (11), 1415–1423.

Nock, W. J., Heaven, S. & Banks, C. J. 2016 Mass transfer and gas–liquid interface properties of single $CO_2$ bubbles rising in tap water. *Chemical Engineering Science* **140**, 171–178.

Perlmutter, D. 1961 Surface-renewal models in mass transfer. *Chemical Engineering Science* **16** (3–4), 287–296.

Shaw, D. A. & Hanratty, T. J. 1977 Turbulent mass transfer rates to a wall for large Schmidt numbers. *AIChE Journal* **23** (1), 28–37.

Shimizu, K., Takada, S., Minekawa, K. & Kawase, Y. 2000 Phenomenological model for bubble column reactors: Prediction of gas hold-ups and volumetric mass transfer coefficients. *Chemical Engineering Journal* **78** (1), 21–28.

Soli, A. L. & Byrne, R. H. 2002 $CO_2$ system hydration and dehydration kinetics and the equilibrium $CO_2/H_2CO_3$ ratio in aqueous NaCl solution. *Marine Chemistry* **78** (2–3), 65–73.

Song, D., Seibert, A. F. & Rochelle, G. T. 2017 Effect of liquid viscosity on mass transfer area and liquid film mass transfer coefficient for GT-OPTIMPAK 250Y. *Energy Procedia* **114**, 2713–2727.

Stoodley, P., Yang, S., Lappin-Scott, H. & Lewandowski, Z. 1997 Relationship between mass transfer coefficient and liquid flow velocity in heterogenous biofilms using microelectrodes and confocal microscopy. *Biotechnology and Bioengineering* **56** (6), 681–688.

Wang, R., Wang, X. & Xiao, F. 2016 Effects of intra-membrane air pressure and liquid-phase flow rate on oxygen mass transfer performance of bubble-free membrane aeration. *China Water Supply and Drainage* **32** (23), 68–71 + 75.

Whitman, W. G. 1923 The two-film theory of gas absorption. *Chemical Metallurgical Engineering* **29**, 146–148.

Xie, W., Jia, S., Luo, H., Luo, W. & Yuan, X. 2022 Experimental study of mass transfer behavior between floating bubbles and liquids in confined space. *Journal of Chemical Engineering* **73** (7), 2902–2911.

Yang, Z., Zhang, Z., Yang, J. & Lu, J. 2022 Oxygen gas-liquid mass transfer characteristics under enhanced ventilation of sewage pipes. *Environmental Science* **43** (4), 2055–2061.


First received 17 December 2023; accepted in revised form 5 April 2024. Available online 15 April 2024